RESEARCH PAPER

Channels 8:1, 62–75; January/February 2014; © 2014 Landes Bioscience

Alternative splice isoforms of small conductance calcium-activated SK2 channels differ in molecular interactions and surface levels

Elizabeth Storer Scholl[1,†], Antonella Pirone[1], Daniel H Cox[1], R Keith Duncan[2], and Michele H Jacob[1,*]

[1]Department of Neuroscience; Tufts University Sackler School of Graduate Biomedical Sciences; Boston, MA USA; [2]Department of Otolaryngology; University of Michigan; Ann Arbor, MI USA

[†]Current affiliation: Department of Molecular Physiology and Biophysics; University of Iowa Carver College of Medicine; Iowa City, IA USA

Keywords: SK channel, nAChR, sensory hair cell, neuron, calcium, calmodulin, olivocochlear, synapse

Abbreviations: nAChR: nicotinic acetylcholine receptor; IHCs, inner hair cells; OHC, outer hair cells; CaM, calmodulin; CaMBD, CaM-binding domain; HC, hippocampus; Ctx, cortex; CICR, Ca^{2+}-induced Ca^{2+} release

Small conductance Ca^{2+}-sensitive potassium (SK2) channels are voltage-independent, Ca^{2+}-activated ion channels that conduct potassium cations and thereby modulate the intrinsic excitability and synaptic transmission of neurons and sensory hair cells. In the cochlea, SK2 channels are functionally coupled to the highly Ca^{2+} permeant α9/10-nicotinic acetylcholine receptors (nAChRs) at olivocochlear postsynaptic sites. SK2 activation leads to outer hair cell hyperpolarization and frequency-selective suppression of afferent sound transmission. These inhibitory responses are essential for normal regulation of sound sensitivity, frequency selectivity, and suppression of background noise. However, little is known about the molecular interactions of these key functional channels. Here we show that SK2 channels co-precipitate with α9/10-nAChRs and with the actin-binding protein α-actinin-1. SK2 alternative splicing, resulting in a 3 amino acid insertion in the intracellular 3' terminus, modulates these interactions. Further, relative abundance of the SK2 splice variants changes during developmental stages of synapse maturation in both the avian cochlea and the mammalian forebrain. Using heterologous cell expression to separately study the 2 distinct isoforms, we show that the variants differ in protein interactions and surface expression levels, and that Ca^{2+} and Ca^{2+}-bound calmodulin differentially regulate their protein interactions. Our findings suggest that the SK2 isoforms may be distinctly modulated by activity-induced Ca^{2+} influx. Alternative splicing of SK2 may serve as a novel mechanism to differentially regulate the maturation and function of olivocochlear and neuronal synapses.

Introduction

SK2 channels are widely expressed in electrically excitable cells of the nervous system, including sensory hair cells, neurons, and muscle.[1-3] They are voltage-independent, Ca^{2+}-activated ion channels that flux potassium cations along their concentration gradient into the extracellular space, thereby hyperpolarizing the membrane potential. They are activated by Ca^{2+} signaling, and affect both intrinsic excitability and synaptic transmission.[4,5] Studies of the cochlea in SK2 knockout mice demonstrate that SK2 is essential in prehearing inner hair cells (IHCs) for proper differentiation and function of afferent synapses onto primary auditory neurons that signal sound reception to the brain.[6,7] SK2 is also required in outer hair cells (OHCs) for the differentiation and maintenance of efferent olivocochlear synapses[8,9]; olivocochlear activation leads to OHC hyperpolarization that suppresses the active mechanical processes by which OHCs amplify auditory signals detected by IHCs.[10-12] Efferent inhibition is critical to normal hearing sensitivity and frequency selectivity[13,14] and may protect the cochlea from noise-induced damage.[15-18]

SK2 tetrameric channels are activated by increases in intracellular Ca^{2+} (sub-micromolar range). The Ca^{2+}-binding protein calmodulin (CaM), which is constitutively associated with the SK2 intracellular C-termini, regulates Ca^{2+} sensing and channel gating.[19] Binding of Ca^{2+} to CaM induces a conformational change in the SK2-CaM complex, which leads to the opening of the channel.[19-21] SK2 channels are functionally coupled to local Ca^{2+} sources in micro- or nanodomains in different cell types, allowing rapid channel activation in response to Ca^{2+} influx.[22] SK2 channels are coupled to voltage-gated Ca^{2+} channels in cardiac muscle, NMDA receptors in neurons, and α9/10-nAChRs in cochlear hair cells.[1,23,24] The molecular mechanisms underlying the close coupling of SK2 channels to their Ca^{2+} source are poorly defined.

*Correspondence to: Michele H Jacob; Email: michele.jacob@tufts.edu
Submitted: 08/14/2013; Revised: 11/26/2013; Accepted: 12/09/2013; Published Online: 01/06/2014
http://dx.doi.org/10.4161/chan.27470

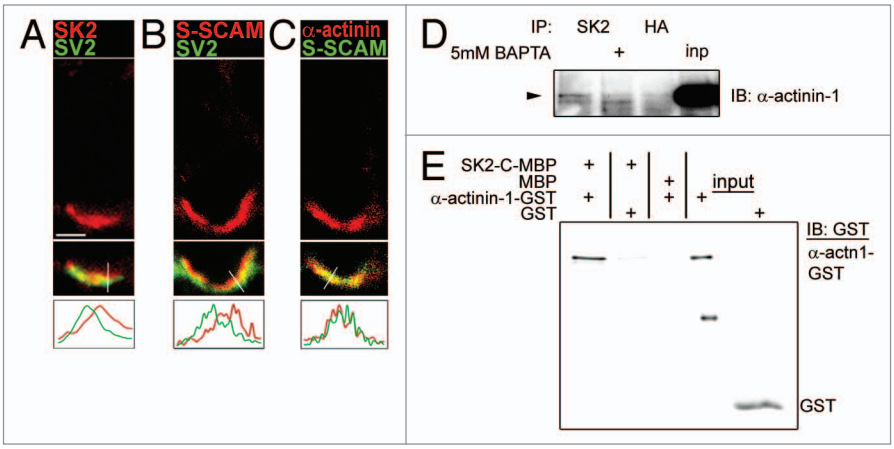

Figure 1. α-actinin localizes to olivocochlear postsynaptic sites in sensory hair cells and interacts with SK2 channels. (**A–C**) Micrographs of fluorescent immunolabeling of E19 chicken hair cells show that SK2 (red, **A**) and the postsynaptic scaffold protein S-SCAM (red, **B**) are predominantly concentrated at olivocochlear postsynaptic sites, based on juxtaposition and partial overlap (yellow) with SV2 labeled presynaptic terminal vesicle clusters (green, **A** and **B**). α-actinin (red, **C**) is also enriched at postsynaptic sites, based on co-localization and strong overlap with S-SCAM (green, **C**). Lower panels: Profiles of pixel intensity peaks show partial overlap of SK2 with SV2 (**A**) and S-SCAM with SV2 (**B**), and almost complete overlap of α-actinin with S-SCAM (**C**). Pixel intensities were measured along a line drawn vertically across the postsynaptic and presynaptic membranes (white lines shown in middle panels). Scale bar = 5μM. (**D**) Co-precipitation of SK2 channels with α-actinin-1 from E20 chicken cochlea lysates, detected by immunoprecipitating (IP) SK2 and immunoblotting (IB) with an anti-α-actinin-1 antibody. Co-IP was seen in the absence and, to a lesser extent, presence of BAPTA (5mM) to chelate Ca^{2+}. In contrast, α-actinin-1 did not co-precipitate with anti-HA antibody, as a negative control. Input, 6% of total lysate. (**E**) Direct binding of recombinant GST-tagged α-actinin-1 with the MBP-tagged SK2 C-terminus (SK2-C). There are no non-specific interactions between SK2 or α-actinin-1 with only GST or MBP, respectively (lanes 2,3). IB; GST antibody. Inputs, 0.5% of total peptide used in IP (lane 4, α-actinin-1-GST; lane 5, GST alone). There is a lower band in lane 4 that is likely a degradation product that does not bind to SK2. (**A–E**) n = 3 separate experiments.

Accumulating evidence suggests that SK2 channels are essential organizers of efferent olivocochlear synapses on OHCs. On normal developing hair cells, the first appearance of SK2 clusters coincides with that of α9/10-nAChR clusters, and synaptic responses to efferent stimulation appear contemporaneously with ACh-evoked SK currents, suggesting that SK2 channels may be required at the onset of synaptic function.[6] Importantly, SK2-null mice exhibit a complete absence of ACh-evoked currents from OHCs, despite normal levels of nAChR subunit mRNAs.[9] Further, efferent presynaptic terminals do form on the SK2 null hair cells during early postnatal development, but subsequently degenerate, demonstrating that SK2 channels are required for their maintenance.[8,9] In comparison, hair cells of α9- and α10-nAChR subunit knockout mice lack cholinergic sensitivity, but retain efferent innervation, albeit with abnormal, hypertrophied bouton morphology.[25,26] Moreover, α9-knockout mice display normal SK2 localization at postsynaptic sites.[8] Taken together, these studies suggest that SK2 channels localize at postsynaptic sites independent of α9/10-nAChRs, whereas SK2 is essential for α9/10-nAChR surface membrane expression and/or function. These findings lead to the suggestion that SK2 may be physically linked to α9/10-nAChRs in a preassembled complex and SK2 thereby directs the intracellular trafficking and surface membrane expression/ stable retention of the receptors.[8,9] Alternatively, SK2 may direct the assembly of a postsynaptic protein complex that is required for surface α9/10-nAChRs to be functional. These data highlight the importance of identifying molecular interactions of SK2 channels.

Several protein binding partners that modulate SK2 surface expression have been identified. Constitutive, Ca^{2+}-independent CaM interactions are required for SK2 surface membrane expression in heterologous cells.[27] In cardiac myocytes, SK2 interacts with α-actinin-2, a member of the α-actinin family of actin cross-linking proteins.[23] This interaction links SK2 to its native Ca^{2+} source, $Ca_v1.3$ channels, and is required for SK2 surface membrane expression in cardiac myocytes and in heterologous cells, suggesting that α-actinin-2-mediated linkage to the actin cytoskeleton may promote SK2 surface membrane insertion and/or stable retention.[23,28] SK2 channels are also constitutively bound to the protein kinase CK2 and the PP2A protein phosphatase, which modulate channel Ca^{2+} sensitivity through regulation of CaM phosphorylation.[29]

Our studies sought to identify molecular interactions of SK2 channels that may function in cochlear hair cells because of the key role of these channels in the organization and function of olivocochlear synapses. We focus on chicken SK2 because alternative splice isoforms have been recently identified but little is known about their specific properties and developmental expression levels.[30] Here, we identify α-actinin-1 as a novel binding partner of SK2 in chicken hair cells. We provide the first demonstration of a physical association between SK2 and α9/10-nAChRs, based on their co-precipitation from heterologous cells. We show developmental regulation of the relative levels of transcripts encoding the SK2 alternative splice variants during stages of synaptic maturation in the embryonic chicken cochlea. Similarly, we demonstrate that mouse hippocampal and cortical neurons also express the SK2 splice variants, and developmentally regulate their levels. Intriguingly, our heterologous expression studies show that the SK2 isoforms exhibit differences in their molecular interactions, surface levels, and regulation by Ca^{2+} and CaM. The differential properties of SK2 splice variants suggest a molecular complexity of SK2 channels at synapses.

Results

SK2 interacts with α-actinin-1 in cochlear hair cells

To begin to define mechanisms of SK2 channel localization and functional coupling to its local Ca^{2+} source in cochlear sensory hair cells, we sought to identify proteins that interact with SK2.

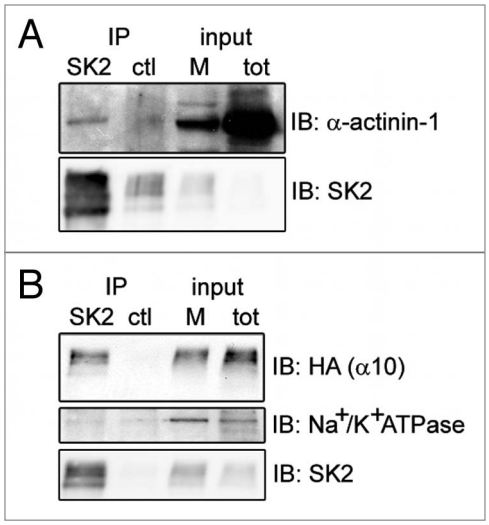

Figure 2. α-actinin-1 and α9/10-nAChRs interact with SK2 channels in *Xenopus* oocytes. Immunoblots show co-precipitation of exogenous SK2 with co-expressed α-actinin-1 (**A**) and HA-tagged α9/10-nAChRs (**B**) in *Xenopus laevis* oocytes. As negative controls, α-actinin-1 and nAChRs did not co-precipitate with an unrelated antibody of the same IgG subclass (anti-mGluR5; ctl lane in **A** and **B**) and SK2 did not co-precipitate with endogenous Na^+/K^+ ATPase (**B**, lower panel). Input, 6% of total membrane fraction (M) and lysate (tot) for all panels. n = 4 separate experiments.

In cardiac muscle, SK2 channels interact with α-actinin-2, which is necessary for surface membrane expression.[23,28] To determine whether α-actinins may interact with SK2 channels in a distinct cell type, inner ear hair cells, we first identified α-actinin isoforms expressed in these cells. We performed reverse-transcription (RT)-PCR with specific primers to amplify α-actinin from total RNA isolated from E19 chicken basilar papillae (equivalent of the mammalian cochlea). The PCR primers were designed against conserved regions flanking the EF-hand region of α-actinin, which differs in each isoform. Sequencing indicated that the α-actinin isoform expressed in the basilar papilla is not α-actinin-2, a muscle-specific, non-Ca^{2+}-sensitive isoform, but a Ca^{2+}-sensitive non-muscle isoform. We tested whether α-actinin localizes at olivocochlear synapses in sensory hair cells in vivo, using a pan-specific α-actinin monoclonal antibody. SK2 is concentrated at these postsynaptic sites, as indicated by the juxtaposition of SK2 immunolabeled surface clusters to the large calyx-type olivocochlear presynaptic terminal, marked by SV2 synaptic vesicle staining (**Fig. 1A**). We were unable to directly demonstrate co-localization of SK2 with α-actinin because of the poor match between optimal fixation conditions for their immunostaining. Instead, we showed that α-actinin, like SK2, is enriched postsynaptically, as indicated by co-localization with the synapse specific cell adhesion molecule (S-SCAM) (**Fig. 1C**; yellow = overlap of the red and green double labeling). S-SCAM is a scaffold protein that is enriched at nicotinic postsynaptic sites in neurons[31] and in sensory hair cells (**Fig. 1B**). These results demonstrate that both α-actinin and SK2 are concentrated postsynaptically at the basal synaptic pole of inner ear hair cells.

Consistent with their co-localization, α-actinin co-immunoprecipitated with SK2 from chicken cochlea membrane fractions (**Fig. 1D**), demonstrating their interaction in vivo. Next, we tested for direct binding of α-actinin-1 to the SK2 C terminus using recombinant peptide binding assays. The MBP-tagged SK2 C-terminus construct pulled down GST-tagged α-actinin-1 (**Fig. 1E**). As tests for specificity, GST alone

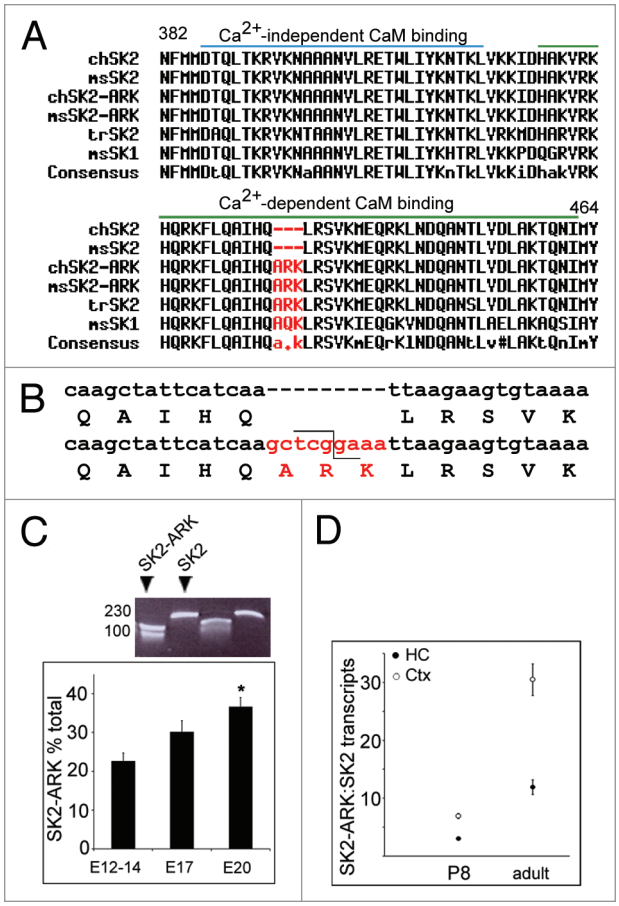

Figure 3. Increases in developmental expression of SK2-ARK splice variant in chicken cochlear hair cells in vivo. (**A**) Sequence alignments of the C-terminus of chicken (ch) splice variants, SK2 and SK2-ARK (24), mouse SK2 (GenBank accession number P58390) and SK2-ARK, trout SK2 (NP_001117783) and mouse SK1 (Q9EQR3). Numbers indicate amino acids of chicken SK2. Source: http://multalin.toulouse.inra.fr/multalin/. (**B**) ARK insertion (lower sequence) creates a unique restriction endonuclease site (Hpy188I) that is not present in chicken SK2 (upper sequence) that lacks the insert. (**C**) Quantification of relative abundance of SK2-ARK mRNA, compared with SK2, during chicken cochlear development, ranging from embryonic day (E)12–14 to E20. Identification of cDNA clones of SK2-ARK (lanes 1,3) and SK2 (lanes 2,4) by using Hpy188I restriction digestion and size separation of the products by agarose gel electrophoresis. The cDNAs were generated by RT-PCR amplification from cochleae total RNA with primers to conserved sequences that flank the ARK insertion site and subcloning (~150 clones analyzed in total per age). Bottom: quantification of the relative abundance of SK2-ARK transcript. n = 3 separate RT-PCR experiments with independent RNA extractions, 50–60 clones per age per experiment. (**D**) Graph of developmental increases in the relative abundance of SK2-ARK transcripts, detected by q-PCR, in the mammalian hippocampus (HC) and cortex (Ctx) from postnatal day 8 to 3 mo of age (adult). n = 6 animals per age, 3 separate q-PCR experiments with independent RNA extractions. Bars and data points in (**C** and **D**) represent mean ± SEM; * $P < 0.01$ Student *t* test compared with levels at E12–14.

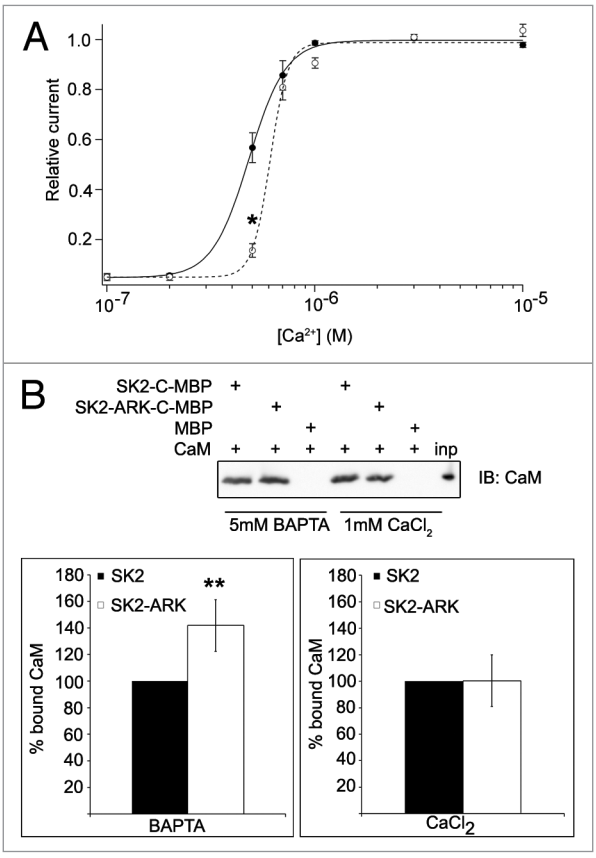

Figure 4. Ca^{2+} gating of SK2 and SK2-ARK channels. (**A**) Mean normalized Ca^{2+} response curves for SK2 (solid line) and SK2-ARK (dashed line) currents recorded in inside-out patches of *Xenopus* oocyte membranes. SK2 and SK2-ARK currents during 50mV voltage steps were recorded in different Ca^{2+} concentrations. Normalized curves were fitted with the Hill equation. * $P < 5 \times 10^{-7}$, Student *t* test; n = 13 for both SK2 and SK2-ARK. (**B**) Recombinant peptide binding assay shows direct binding of CaM to MBP-tagged SK2 and SK2-ARK C-termini in the presence of 5mM BAPTA or 1mM $CaCl_2$. Input, 1% of CaM used in pulldown. Histograms show band densities of co-precipitated CaM normalized to SK2-C-MBP or SK2-ARK-C-MBP in each lane (detected with anti-MBP antibody). In each experiment, normalized levels of CaM co-precipitated with SK2-ARK-MBP were calculated as a percentage of CaM co-precipitation with SK2-MBP (100%). Bars represent mean percentage ± SEM ** 95% confidence interval was 103.73–179.95% of SK2 values. n = 3 separate experiments.

did not co-precipitate with SK2-C-MBP, and MBP alone did not co-precipitate α-actinin-1-GST. Taken together, our results show that α-actinin-1 interacts directly with SK2 channels and both localize at postsynaptic sites in chicken cochlear hair cells in vivo.

SK2 interacts with α9/10-nAChRs

Proper function of olivocochlear synapses on hair cells requires close physical proximity (co-localization) and functional coupling of SK2 channels with α9/10-nAChRs,[1,6] but a physical association has not been demonstrated to date. To test for their interaction, we utilized heterologous expression in *Xenopus laevis* oocytes, rather than the native proteins in hair cells, because of the lack of reliable antibodies that recognize α9- and α10-nAChR subunits. We epitope tagged the chicken α10-nAChR subunit C-terminus end with hemagglutinin (HA). Oocytes were microinjected with cRNA encoding α9, α10-HA, SK2, and α-actinin-1. SK2 channels were immunoprecipitated from membrane fractions isolated from oocytes three days after injection, the time determined experimentally to provide optimal expression levels. As a positive control, exogenously expressed SK2 co-precipitated with α-actinin-1 from oocyte membrane fractions (**Fig. 2A**), consistent with the co-precipitation of these endogenous proteins from cochlear lysates (**Fig. 1D**). Importantly, SK2 channels co-precipitated with HA-tagged α9/10-nAChRs (**Fig. 2B**). The interaction is specific, as SK2 did not co-precipitate with other membrane proteins, such as the endogenous sodium potassium ATPase (**Fig. 2B**). As an additional negative control, SK2 antibody did not pull down HA-tagged α9/10-nAChRs from oocytes not co-expressing exogenous SK2 (see **Fig. 5A**). This is the first demonstration, to our knowledge, of a physical association between SK2 and α9/10-nAChRs.

Expression of SK2 splice variants during chicken embryonic development

Previous studies of posthatch chicken short (outer) hair cells identified an SK2 splice variant, containing a 3-residue "ARK" insertion within the C terminus (**Fig. 3A**), referred to here as SK2-ARK.[30] We and others have also detected the ARK splice insertion in mammalian SK2.[32] The same insertion is constitutively present in trout SK2, and a similar AQK sequence is found in the same region in mammalian SK1 (**Fig. 3A**).[30] Because the ARK insertion localizes to the domain that binds CaM, a protein that regulates SK2 surface expression and Ca^{2+}-gating, we speculated that SK2 isoforms may exhibit differences in protein interactions and functional properties.

First, we determined whether SK2-ARK is expressed during the period of olivocochlear synapse formation, from E12-E20, in the embryonic chicken cochlea. To quantify the relative abundance of SK2 (refers here to the isoform that lacks the ARK insert) and SK2-ARK transcripts, we used RT-PCR with specific primers that flanked the splice insertion site, followed by subcloning and restriction endonuclease digestion of individual clones with Hpy188I, a restriction endonuclease that cuts at a unique site within the sequence encoding the ARK splice insertion, but not in SK2 lacking the insert (**Fig. 3B and C**). From the 150–180 clones analyzed for each developmental age, we found a significant increase in the relative abundance of the SK2-ARK variant between ages E12-E14 and E20 (**Fig. 3C**; 22.69 ± 4.01% of SK2 clones at E12–14; 36.63 ± 4.21% at E20, n = 3 separate experiments with 50–60 clones per experiment, $P < 0.01$, Student *t* test).

In addition, SK2-ARK transcripts show a substantial developmental increase in mouse forebrain regions. The relative levels of SK2-ARK to SK2 transcripts increased by approximately 4-fold in both the hippocampus (2.9 ± 0.2; 11.9 ± 1.3; n = 6) and the cortex (6.9 ± 0.4; 30.5 ± 2.7 n = 6) from postnatal day 8 to adult ages (3 mo) (**Fig. 3D**). Thus, cochlear sensory hair cells and central neurons both exhibit increases in the relative levels of SK2 containing the ARK insertion. The chicken, mouse and human SK2 clones are 89% identical in sequence (**Fig. 3A**), suggesting that they are likely

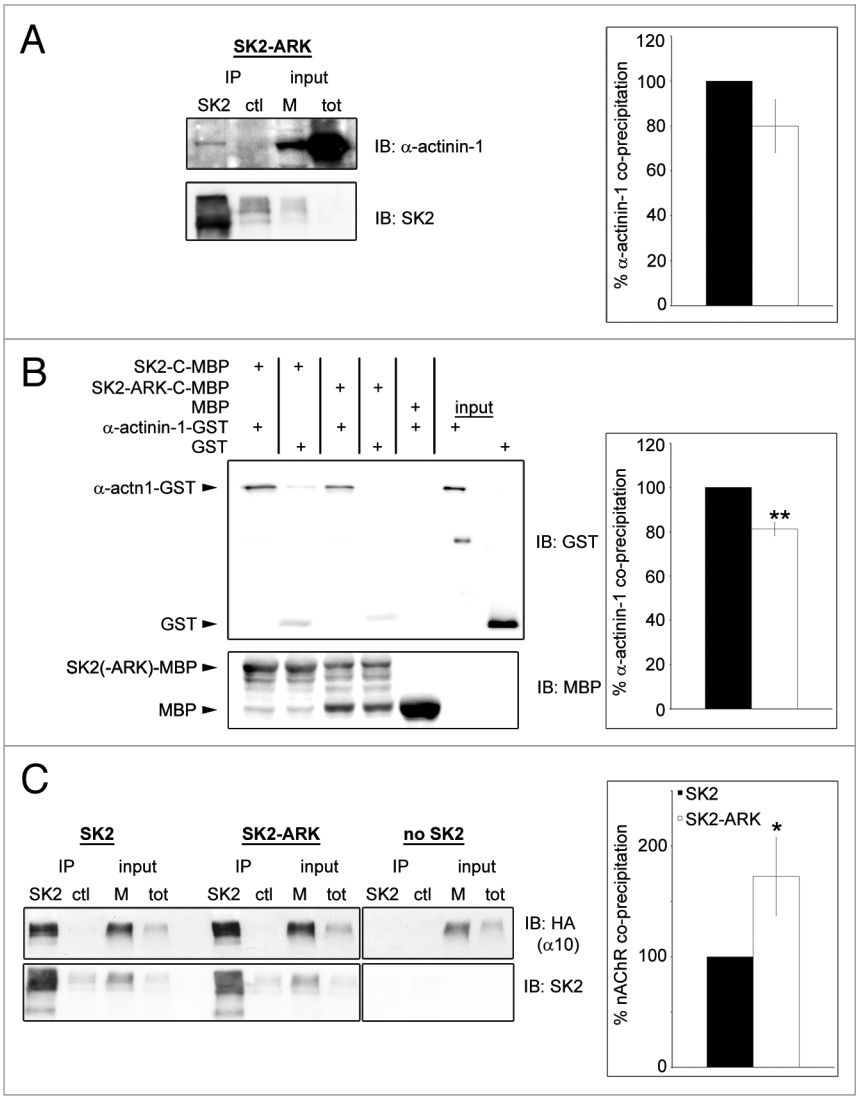

Figure 5. ARK alternative splicing alters interactions of SK2 with α9/10-nAChRs and α-actinin-1. Co-immunoprecipitation of α -actinin-1 (**A**; see also **Fig. 2A**) and HA-tagged α9/10-nAChRs (**C**) with SK2 and SK2-ARK exogenously expressed in *Xenopus* oocytes. (**A** and **C**) Negative controls show no α-actinin-1 or α9/10-nAChR co-precipitation with an unrelated antibody (ctl lanes) or (**C**) with SK2 antibody from oocytes not transfected with exogeneous SK2. Input in (**A** and **C**), 6% of total membrane fraction (M) and lysate (tot). (**B**) Direct interactions of GST-tagged α -actinin-1 with MBP-tagged SK2 or SK2-ARK C-termini. IP: MBP antibody to pull down SK2, IB: GST antibody. Negative controls show little or no nonspecific interactions with MBP or GST alone (lanes 2,4,5). Input, 0.5% of GST-α-actinin-1 and GST used in pulldown. The lower band in lane 6 is likely a degradation product. (**A**–**C**) Graphs show normalized band densities of co-precipitated proteins relative to precipitated SK2 or MBP-tagged SK2 or SK2-ARK peptide in each lane. In each experiment, normalized protein levels co-precipitated with SK2-ARK were calculated as a percentage of co-precipitation with SK2 (100%). Bars represent mean percentage ± SEM * 95% confidence interval was 103.83–241.27% of SK2 values. ** 99.99% confidence interval was 70.00–92.50% of SK2 values. n = 4 separate experiments (**A**) and 3 separate experiments (**B** and **C**).

to have conserved molecular interactions. Similarly, the chicken α-actinin-1 amino acid sequence is 97% homologous to human α-actinin-1.[33,34]

Functional characterization of the SK2-ARK isoform

We tested for differential properties between SK2 and SK2-ARK in order to gain insights into the functional significance of the increased developmental expression of SK2-ARK. We utilized heterologous expression in *Xenopus laevis* oocytes because: (1) no reagents are available to distinguish between the two SK2 isoforms, which differ by only 3 amino acids and (2) exogenous SK2 forms functional channels on the oocyte surface.[4] Since the ARK splice insertion is located within the Ca^{2+}-dependent CaM binding domain of the SK2 C-terminus, we tested for effects on CaM-mediated Ca^{2+} gating. We used patch-clamp recording to look for differences in Ca^{2+} sensitivity between channels composed of SK2-ARK vs. SK2 subunits. SK2 and SK2-ARK isoforms were separately expressed in oocytes, and Ca^{2+} responses were recorded from inside-out patches to generate Ca^{2+} dose-response curves. Ca^{2+}-activated potassium currents recorded from SK2-expressing patches had an apparent KD of 0.48 ± 0.0067 μM and a Hill coefficient of 4.90 ± 0.40 (n = 13). SK2-ARK channels demonstrated a steeper, right-shifted Ca^{2+} response curve caused by a significantly reduced normalized response to 0.5 μM Ca^{2+}, with an increased apparent KD of 0.61 ± 0.019 μM and a Hill coefficient of 10.14 ± 1.84 (**Fig. 4A, n** = 13). These results demonstrate that the ARK insertion alters the response of the assembled channels to Ca^{2+}, which could suggest altered interactions with CaM.

To assess this possibility, we tested for differences in CaM binding to SK2 and SK2-ARK C-termini in recombinant peptide binding assays. We found no difference in binding of Ca^{2+}-bound CaM between the two isoforms (**Fig. 4B**). In contrast, we observed a modest significant increase in binding of SK2-ARK to CaM when Ca^{2+} was chelated with 5mM BAPTA (**Fig. 4B**, 141.84 ± 19.44% co-precipitated CaM compared with SK2; n = 3). Our results demonstrate that the ARK splice insertion alters both SK2 interactions with CaM and sensitivity to Ca^{2+}.

SK2 ARK splice insertion modulates interactions with α9/10-nAChRs and surface levels

Native SK2 channels interact with α-actinin-1 (**Fig. 1D**), and recombinant SK2 (lacking the ARK insert) interacts with both α-actinin-1 and α9/10-nAChRs (**Figs. 1E and 2B**). We next tested whether the ARK splice insertion affects these interactions.

SK2-ARK or SK2 was co-expressed with exogenous α-actinin-1 in oocytes and immunoprecipitated from membrane fractions. SK2-ARK also co-precipitated with α-actinin-1 from oocyte membranes (**Fig. 5A**; n = 3) but displayed decreased

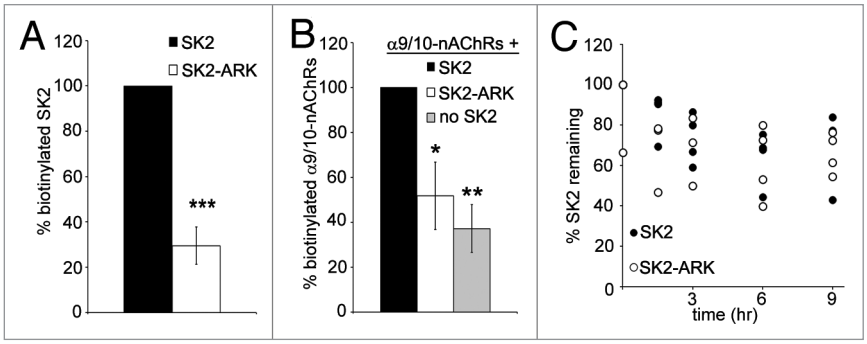

Figure 6. Surface membrane levels of SK2, SK2-ARK, and α9/10-nAChRs. (**A**) Histogram of SK2 and SK2-ARK surface levels, normalized biotinylated band densities at time 0 (precipitation immediately following biotinylation). (**B**) Histogram of α9/10-nAChRs surface levels expressed alone, or co-expressed with SK2, or SK2-ARK, all with α-actinin-1, normalized band densities at time 0. (**C**) Graph of the remaining surface levels of biotinylated SK2 or SK2-ARK at indicated time points relative to levels at time 0, indicating their relative stability in the surface membrane. Graphs indicate band densities of precipitated SK2 or nAChRs normalized to input membrane expression. In each experiment, normalized levels of biotinylated SK2-ARK (**A**) or nAChRs co-expressed with SK2-ARK or no SK2 (**B**) were calculated as a percentage of biotinylated SK2 or nAChRs co-expressed with SK2 (100%). In each experiment (**C**), remaining levels of biotinylated SK2 or SK2-ARK were calculated as a percentage of biotinylated levels at time 0. Bars represent mean ± SEM * 99.5% confidence interval was 9.64–93.78% of co-expression with SK2. ** 99.99% confidence interval was -4.14–78.45% of co-expression with SK2. *** 99.99% confidence interval was -2.47–61.41% of SK2 values. n = 5 separate experiments (**A**) and 3–4 separate experiments (**B** and **C**).

binding to α-actinin-1 in recombinant peptide binding assays (**Fig. 5B**, 81.25 ± 2.89% bound α-actinin-1 compared with SK2; n = 3), suggesting that the ARK splice insertion may modulate SK2 channel interactions with α-actinin-1.

Intriguingly, SK2-ARK showed a significant increase in co-precipitation with α9/10-nAChRs (**Fig. 5C**, 172.55 ± 35.06% compared with SK2; n = 4). SK2 null mouse studies suggest that SK2 is required for surface expression and/or stable retention of α9/10-nAChRs on cochlear hair cells.[8,9] Thus, the difference that we found in their co-precipitation with α9/10-nAChRs (**Fig. 5C**) raises the possibility that the SK2 isoforms may have differential effects on nAChR trafficking.

We therefore tested for differences in surface membrane levels of α9/10-nAChRs co-expressed with either SK2-ARK or SK2 in oocytes. We used standard cell surface biotinylation assays with a membrane-impermeant biotinylation reagent. For each protein of interest, the levels on the surface (biotinylated) were normalized to their total expression levels. The two SK2 isoforms displayed similar total expression levels; however their surface levels differed. SK2-ARK surface levels were dramatically reduced, 29.47 ± 8.21% compared with SK2 levels (**Fig. 6A**; n = 5).

Consistent with the SK2 null mouse studies that suggest co-trafficking, α9/10-nAChR surface levels were significantly lower when expressed alone compared with co-expression with SK2 (**Fig. 6B**, 37.16 ± 10.61% of surface levels co-expressed with SK2, n = 3–4). Unexpectedly, α9/10-nAChR surface levels were not different when expressed alone vs. co-expressed with SK2-ARK, suggesting that SK2-ARK, in sharp contrast to SK2, does not augment receptor surface levels. α9/10-nAChR surface levels were 50% lower with SK2-ARK vs. SK2 (**Fig. 6B, n** = 3–4), whereas the receptors exhibited increased co-precipitation with SK2-ARK from total membrane fractions (**Fig. 5A**). These findings suggest that receptor association with SK2-ARK, compared with SK2, leads to their greater intracellular localization. In summary, SK2-ARK, compared with SK2, exhibits reduced association with α-actinin-1 (**Fig. 5B**), and greater association with α9/10-nAChRs (**Fig. 5C**).

Based on the reduced SK2-ARK surface levels, we tested for increased turnover by measuring retention of the biotinylated protein on the cell surface over time after labeling. The 2 isoforms showed similar rates of endocytosis, as evidenced by similar percentages of initial surface biotinylated SK2 and SK2-ARK that remained at several time points after labeling (**Fig. 6C**). Thus, although surface membrane insertion of SK2-ARK is reduced compared with SK2, the 2 isoforms display similar surface stability (**Fig. 6A and C**). Taken together, our findings indicate that alternative splicing of SK2 likely modulates surface levels and ability to facilitate α9/10-nAChR surface membrane expression.

SK2 interactions are regulated by Ca^{2+} and calmodulin

Ca^{2+} is a key regulator of SK2 channel activation. Increases in local Ca^{2+} concentration induced by synaptic activity lead to Ca^{2+}-dependent binding of CaM to the Ca^{2+}-dependent CaM binding domain (CaMBD) of an adjacent SK2 subunit, resulting in conformational changes that mediate channel gating.[19-21] The ARK insert is located within the CaMBD of SK2 (**Fig. 3A**), suggesting the possibility that Ca^{2+} and CaM interactions with the different SK2 isoforms will exhibit differential modulation. In particular, Ca^{2+} and CaM may affect interactions of SK2 channels with the actin binding protein α-actinin-1 and with the Ca^{2+}-permeant α9/10-nAChRs. As support for this hypothesis, α-actinin-2 interacts with the CaMBD of SK2 from cardiac muscle,[23,28] and α-actinin-1 interactions with the NMDAR NR1 subunit are inhibited by Ca^{2+}-bound CaM.[35]

We tested first for effects of Ca^{2+} alone on the binding of α-actinin-1 to SK2 and SK2-ARK using recombinant peptide binding assays. Ca^{2+} strongly promoted α-actinin-1 binding; we found a 3.2-fold increase in binding of α-actinin-1 to SK2 and a 6.8-fold increase in binding to SK2-ARK in the presence of 1mM $CaCl_2$, compared with 5mM BAPTA (**Fig. 7A**; compare lanes 1 and 3, 5 and 7 with no CaM; n = 3). Similarly, α-actinin-1 co-precipitation with SK2 was reduced by loading oocytes with BAPTA-AM to chelate intracellular Ca^{2+} prior to SK2 immunoprecipitation (**Fig. 7B**; 78.72 ± 9.98% compared with untreated controls; n = 3). These data suggest that increased intracellular Ca^{2+} levels likely strengthen α-actinin-1 interactions with both SK2 and SK2-ARK subunits. Such

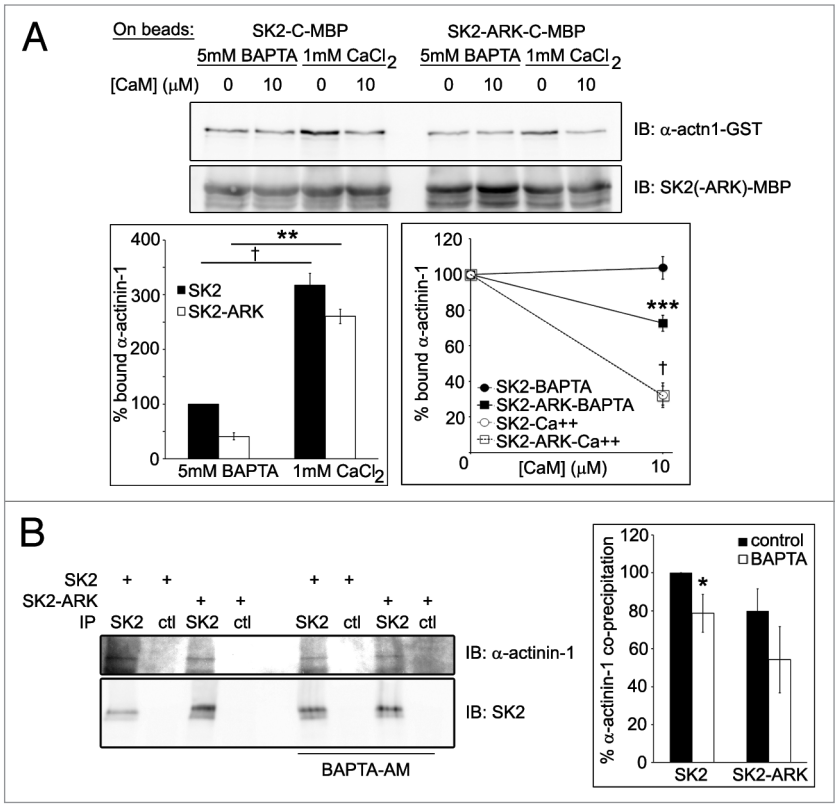

Figure 7. Ca^{2+} and CaM modulate interactions of SK2 and SK2-ARK with α-actinin-1. (**A**) Recombinant peptide binding assays showing effects of Ca^{2+} and CaM on binding of α-actinin-1 to SK2 and SK2-ARK. Purified recombinant CaM at the indicated concentrations was incubated with equal amounts of MBP-tagged SK2 or SK2-ARK C-terminus constructs and amylose beads in buffer containing 5mM BAPTA or 1mM $CaCl_2$ prior to incubation with GST-tagged α-actinin-1. Immunoblots and graph (lower left) show that elevated Ca^{2+} (buffer containing 1mM $CaCl_2$) increases the levels of GST-tagged α-actinin-1 bound to SK2 and SK2-ARK C-terminal peptides, compared with low Ca^{2+} (buffer containing 5mM BAPTA). Immunoblots and graph (lower right) show that CaM, in the presence of Ca^{2+} decreases the amount of α-actinin-1 bound to both isoformsbut only to SK2-ARK in the absence of Ca^{2+} (**B**) Immunoblots and graph show decreased co-precipitation of exogenous α-actinin-1 with SK2 and SK2-ARK from oocytes incubated with BAPTA-AM (10mM) to chelate intracellular Ca^{2+} prior to and during lysis. All graphs show normalized band densities of bound α-actinin-1-GST (**A**) or α-actinin-1 (**B**) normalized to MBP-tagged SK2 construct or SK2 in each lane. In each experiment, normalized protein levels co-precipitated with SK2-ARK were calculated as a percentage of co-precipitation with SK2 (100%). Bars represent mean ± SEM * 95% confidence interval was 59.15–98.29% of SK2 values with BAPTA. ** $P < 0.0005$ Students *t* test; † 99.99% confidence interval was 234.91–400.48% of SK2 values with BAPTA. *** 99.99% confidence interval was 55.21–90.01% of SK2-ARK values with 10 μM CaM; † 99.99% confidence intervals were 5.27–59.20% of SK2 values and 11.43–52.56% of SK2-ARK values with 10 μM CaM. n = 3 separate experiments (**A** and **B**).

changes may occur upon olivocochlear synaptic activation in sensory hair cells.

Because CaM exhibits both Ca^{2+}-dependent and independent binding to SK2, we tested whether CaM, in the presence or absence of Ca^{2+}, alters α-actinin-1 interactions with SK2 isoforms. To test for competition between the interactors, we preincubated recombinant SK2 isoforms with CaM in buffer containing either 1mM $CaCl_2$ or 5mM BAPTA, and then measured the binding of α-actinin-1. Preincubation of the SK2 isoforms with Ca^{2+}-bound CaM partially blocked α-actinin-1 binding (**Fig. 7A**; n = 3). Further, Ca^{2+}-free CaM (with 5mM BAPTA) did not affect α-actinin-1 binding to SK2, suggesting that, at low levels of Ca^{2+}, CaM and α-actinin-1 may bind simultaneously to this isoform. In contrast, Ca^{2+}-free CaM partially blocked binding of α-actinin-1 to SK2-ARK (**Fig. 7A**, 72.61 ± 4.47% α-actinin-1 bound in the presence of CaM compared with CaM-free control; n = 3). This result is consistent with our findings that Ca^{2+}-free CaM shows increased binding to SK2-ARK, compared with SK2 (**Fig. 4B**). Thus, Ca^{2+}-independent CaM binding may induce differences in the conformation of SK2-ARK vs. SK2 that, in turn, lead to differential modulation of their interactions with α-actinin-1.

Interestingly, SK2 and SK2-ARK showed different effects of Ca^{2+} chelation on interactions with α9/10-nAChRs. Co-precipitation of α9/10-nAChRs with SK2 from oocytes increased 2-fold after treating with BAPTA-AM (**Fig. 8**; n = 4), suggesting that Ca^{2+} influx may reduce linkage of SK2 to α9/10-nAChRs. In contrast, co-precipitation of α9/10-nAChRs with SK2-ARK was not significantly altered in response to BAPTA-AM treatment, suggesting that Ca^{2+} does not inhibit the association of α9/10-nAChRs with SK2-ARK. These findings suggest that the isoform composition of SK2 channels may provide a novel mechanism for modulating protein interactions at the SK2 postsynaptic complex in response to synaptic activity-induced increases in local Ca^{2+} and Ca^{2+}-CaM binding.

Discussion

Our findings provide novel insights into molecular interactions of SK2 channels and the differential properties of SK2 alternative splice variants. We show that SK2 co-precipitates with α9/10-nAChRs, using heterologous expression. This is the first demonstration, to our knowledge, of a physical association between these 2 key functional channels of olivocochlear postsynaptic sites. Further, we show direct binding of SK2 to the actin-binding protein α-actinin-1 in vitro and in vivo. We also find developmentally regulated expression of SK2 splice variants, in vivo, in the avian cochlea and the mammalian cortex and hippocampus, suggesting widespread significance of SK2 molecular heterogeneity. The SK2-ARK isoform has been identified previously in the avian cochlea,[30] but changes induced by the insert have not been defined prior to our study. We demonstrate that the two isoforms differ in surface membrane levels, interactions with α9/10-nAChRs, Ca^{2+} sensitivity, and modulation of their molecular interactions by Ca^{2+} and calmodulin (**Fig. 9**). Based on these differences, we speculate that the 2 SK2 isoforms provide an unanticipated complexity that may serve to differentially modulate

responses to synaptic activity in sensory hair cells and neurons.

Normal sound sensitivity and frequency selectivity requires the functional coupling and co-localization of α9/10-nAChRs and SK2 channels at efferent olivocochlear postsynaptic sites.[1,36] α9/10-nAChRs mediate efferent olivocochlear synaptic transmission. Activation of these highly Ca^{2+} permeant receptors causes Ca^{2+} influx that, in turn, leads to SK2 channel activation and fast efferent inhibition in both avian and mammalian hair cells.[1,37,38] SK2-null mouse studies demonstrate that these channels play key roles in the organization and function of olivocochlear synapses. In particular, the loss of functional α9/10-nAChRs on the surface of SK2-null hair cells, despite normal levels of receptor subunit mRNAs, suggests that SK2 may interact with the nAChRs in a molecular complex whose surface membrane expression is directed by SK2-specific mechanisms or binding partners.[6,8,9] Consistent with this hypothesis, we show that SK2 channels co-precipitate with α9/10-nAChRs. Whether the interaction is direct or mediated via linker proteins has yet to be determined. Additionally, we demonstrate that the surface levels of α9/10-nAChRs correlates with that of SK2 in heterologous cells, further supporting the model in which surface membrane targeting and/or stable retention of α9/10-nAChRs is promoted by their physical association with SK2.

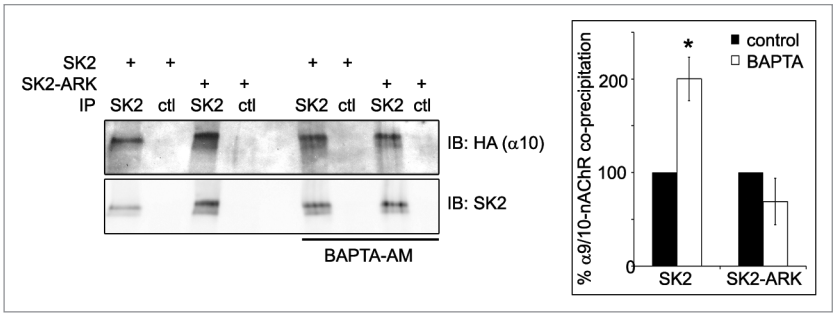

Figure 8. Ca^{2+} differentially modulates interactions of SK2 and SK2-ARK with α9/10-nAChRs. Immunoblots show that incubation with BAPTA-AM (10mM) to chelate intracellular Ca^{2+} leads to increased co-precipitation of HA-tagged α9/10-nAChRs with SK2, but not with SK2-ARK, from oocytes. Graph shows normalized band densities of co-precipitated α9/10-nAChRs relative to precipitated SK2 in each lane. In each experiment, normalized nAChR levels co-precipitated with SK2-ARK were calculated as a percentage of co-precipitation with SK2 (100%). Bars represent mean ± SEM * 99.99% confidence interval was 109.34–290.84% of control SK2 values. n = 4 separate experiments.

SK2 channels in cochlear hair cells may also be activated by increased Ca^{2+}-induced Ca^{2+} release (CICR) from internal stores following nAChR activation. Local Ca^{2+} levels are thought to be tightly regulated and physically restricted by the subsynaptic cistern that lies closely opposed to the postsynaptic membrane.[39-41] In previous studies, blockade of CICR by application of 100 mM ryanodine reduced the amplitude of ACh-evoked IPSCs in hair cells, suggesting that CICR is important for SK2 channel activation.[39] Intriguingly, our findings of Ca^{2+}-induced changes in SK2 isoform interactions with α-actinin-1, which links to the submembranous actin cytoskeleton, suggest that changes in local Ca^{2+} levels may alter the membrane stability or subcellular localization of SK2 channels. Our demonstration of a physical association between α9/10-nAChRs and SK2 channels suggests that both direct coupling to nAChRs and CICR likely mediate Ca^{2+} activation of SK2 channels that, in turn, is required for fast suppression of hair cell-mediated sound amplification, and to promote slow suppression of outer hair cell mechanics that protects against noise-induced hearing loss.[41-43]

SK2 alternative splicing appears to modulate the interactions and surface levels of the SK2-nAChR complex in our heterologous expression studies. We find increased interaction of α9/10-nAChRs with SK2-ARK, relative to SK2. Surface membrane levels of the SK2-ARK variant were significantly reduced compared with SK2. Surface levels of α9/10-nAChRs were also decreased when co-expressed with SK2-ARK, vs. SK2, indicating the dependence of α9/10-nAChR trafficking on that of the SK2 isoforms.

Mechanisms that mediate the trafficking of the SK2-nAChR complex are undefined. SK2 interactions with α-actinin-1 may regulate its surface expression. As support for this hypothesis, cardiac muscle SK2 surface expression and endocytic recycling are affected by interaction with α-actinin-2.[23,28] Our findings of reduced binding of SK2-ARK, compared with SK2, with α-actinin-1 and decreased SK2-ARK surface levels, raise the possibility that α-actinin-1 may play a similar role in the cochlea to that of α-actinin-2 in cardiac muscle, promoting SK2 surface membrane expression and/or stable retention. Interestingly, α-actinin-1 contains EF-hand domains that bind Ca^{2+}. In contrast, α-actinin-2 EF hands do not.[44] Consistent with this difference, we find Ca^{2+}-dependent modulation of SK2 interactions with α-actinin-1. This differs from the reported lack of Ca^{2+} effects on α-actinin-2 interactions with SK2.[28]

We show that Ca^{2+} and CaM modulate SK2 interactions with α9/10-nAChRs and α-actinin-1. Ca^{2+} decreases the association of SK2 with α9/10-nAChRs. Further, Ca^{2+} and Ca^{2+}-bound CaM exert opposing effects on SK2 interaction with α-actinin-1. Ca^{2+} alone strongly promotes SK2 interaction with α-actinin-1. In contrast, Ca^{2+}-CaM, but not Ca^{2+}-free CaM, competes with α-actinin-1 for binding to the SK2 C-terminus, suggesting that the Ca^{2+}-dependent CaMBD is the key region in SK2 for α-actinin-1 binding. Based on these findings, we propose that the balance between Ca^{2+}-CaM-induced displacement vs. Ca^{2+}-mediated enhancement of α-actinin-1 binding to SK2 may shift, depending on local Ca^{2+} concentrations, to increase or decrease SK2 interactions with α-actinin-1. Thus, synaptic activity may lead to local increases in Ca^{2+} that dynamically alter interactions within the SK2-nAChR postsynaptic molecular complex of cochlear hair cells.

The SK2-ARK splice insertion within the Ca^{2+}-dependent CaMBD changes the effects of Ca^{2+} and CaM on SK2 interactions with its binding partners. Ca^{2+}-free CaM showed an increased interaction with SK2-ARK, compared with SK2, and reduced the

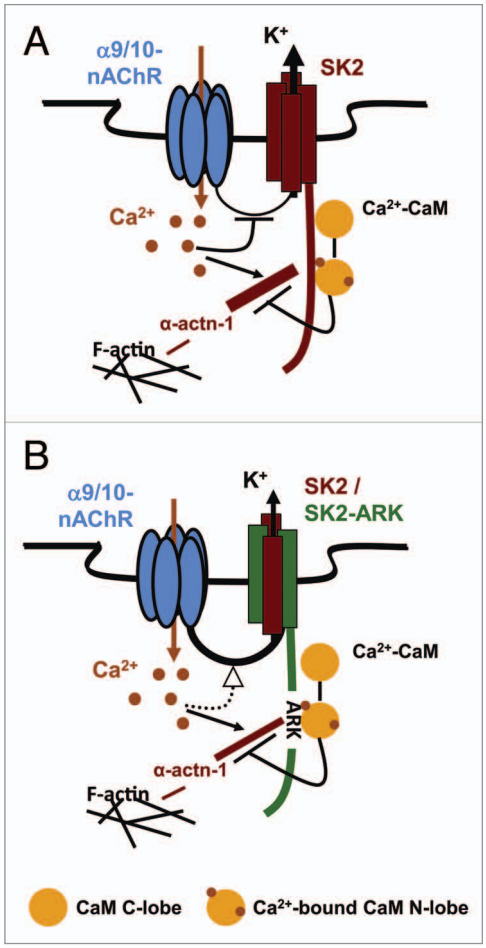

Figure 9. Summary model of the effects of SK2 alternative splicing and Ca^{2+} signaling on the α9/10-nAChR-SK2 channel postsynaptic complex. The model indicates that SK2 channels and α9/10-nAChRs physically interact within a multi-molecular complex that includes the actin-binding protein α-actinin-1 and that Ca^{2+} modulates the interactions. SK2-ARK, compared with SK2, channels exhibit reduced binding to α-actinin-1, and increased association with α9/10-nAChRs. However, SK2-ARK surface membrane levels are lower than those of SK2. Interactions between α-actinin-1 and SK2 (**A**) and SK2-ARK (**B**) are similarly modulated by Ca^{2+} (enhanced, arrow) and Ca^{2+}-CaM (reduced). Ca^{2+} decreases SK2 interactions with α9/10-nAChRs, possibly serving as a mechanism to regulate efferent inhibition. In comparison, Ca^{2+} does not alter or modestly enhances the SK2-ARK::α9/10-nAChR interactions (dotted arrow), suggesting that they are less prone to inhibition by Ca^{2+}. Additional differences, such as Ca^{2+} sensitivity (see text), suggest that developmental increases in SK2-ARK relative levels may modulate synaptic activity in cochlear hair cells and neurons.

binding of α-actinin-1 to SK2-ARK in peptide binding assays, suggesting that the ARK insert may introduce conformational changes within the CaMBD that favor interaction with CaM over α-actinin-1. Competition by CaM for binding of α-actinin-1 to SK2-ARK may thereby reduce the linkage of SK2-ARK channels to the local actin cytoskeleton and thus results in reduced surface membrane levels of the SK2-ARK variant and of α9/10-nAChRs co-expressed with SK2-ARK. In addition, Ca^{2+} differentially affects the interaction of SK2-ARK vs. SK2 with α9/10-nAChRs. Ca^{2+} inhibits SK2 interactions with α9/10-nAChRs, whereas it has little effect or weakly promotes the association of α9/10-nAChRs with SK2-ARK. These findings indicate that the physical coupling of α9/10-nAChRs to SK2-ARK, compared with SK2, is less prone to inhibition by Ca^{2+}, which may be an important property as olivocochlear synapses mature.

We also demonstrate a modest but significant decrease in Ca^{2+} sensitivity (shift in the Ca^{2+} response curve) of SK2-ARK- vs. SK2-mediated potassium currents. Consistent with our findings, a recent report shows that mammalian SK2-ARK currents are less sensitive to Ca^{2+}.[32] The increased steepness of the Ca^{2+} dose response curve for SK2-ARK compared with SK2 (**Fig. 4A**) suggests that SK2-ARK containing channels respond in a more all-or-none manner, compared with the more graded responses of SK2 channels, to changes in local Ca^{2+} concentrations. Previous studies found similar Ca^{2+}-sensitivity between mammalian SK2 channels, which lack the ARK splice insertion, and SK1 channels with an AQK insert at the same position as ARK in avian SK2.[30] It will be interesting to test whether the differences in charge of the amino acids inserted, neutral glutamine (Q) vs. positively charged arginine (R) may underlie the differential effects of AQK vs. ARK insertion on the modulation of Ca^{2+} sensitivity.

SK channels function as tetramers, either homomers or heteromers composed of different subunits. Since SK1–3 subunits can co-assemble to form functional heterotetramers,[45] it seems likely that SK2 and SK2-ARK may also co-assemble into functional channels. SK2-ARK mRNA levels show developmental increases that are modest in the avian embryonic cochlea and substantial (4-fold) in the mammalian postnatal hippocampus and cortex. Based on the 23 to 37% increases in SK2-ARK transcripts in the cochlea from E12-E14 to E20, equal rates of mRNA translation and subunit co-assembly could potentially result in 60–80% of the channels containing at least one SK2-ARK subunit. The impact of ARK expression and population effects are important issues but are difficult to resolve and interpretation of results will be limited because of the lack of reagents that can distinguish between the SK2 and SK2-ARK isoforms. We lack information about protein expression levels, subunit co-assembly, post-translational modifications, trafficking, and localization in sensory hair cells and neurons. Regulatory effects of ARK on these properties would enhance the importance of its developmental expression changes. Intriguingly, the ARK insertion is immediately adjacent to a predicted phosphorylation site.[50] It will be important for future studies to also define mechanisms that regulate the extent of splicing and whether the relative levels are modified by synaptic activity in cochlear hair cells and forebrain neurons.

Overall, our data suggest that SK2 alternative splicing serves as a novel mechanism for regulating SK2 channel protein interactions, surface levels, and response to Ca^{2+} and CaM. Developmental increases in SK2-ARK levels in vivo during embryonic cochlea hair cell synapse maturation (**Fig. 3C**) raise the possibility that alternative splice isoforms may play a role in modulating hair cell inhibitory responses. By altering the relative levels of SK2 and SK2-ARK during development, and possibly during plasticity in adults, cochlear hair cells may modulate the surface levels and functional coupling of α9/10-nAChRs and SK2

channels, and thereby fine-tune the strength and efficiency of olivocochlear synaptic transmission that leads to hair cell hyperpolarization and suppression of afferent auditory transmission. Our demonstration of SK2-ARK expression in mammalian neurons suggests that the mechanisms uncovered here for avian SK2 channels may have widespread relevance to the mammalian nervous system. This complexity of SK2 isoforms may provide a global mechanism for activity-dependent changes in synaptic function.

Materials and Methods

Antibodies

Primary antibodies used were: monoclonal anti-α-actinin (Sigma, http://www.sigmaaldrich.com/catalog/product/sigma/a5044?lang=en&region=US); monoclonal anti-α-actinin-1 (United States Biological, http://www.usbio.net/item/A0761-01C?highlight); polyclonal anti-MAGI-2/S-SCAM (Sigma, http://www.sigmaaldrich.com/catalog/product/sigma/m2441?lang=en&region=US); polyclonal anti-SK2 potassium channel (Sigma, http://www.sigmaaldrich.com/catalog/product/sigma/p0483?lang=en&region=US); monoclonal anti-SV2 (Developmental Studies Hybridoma Bank, http://dshb.biology.uiowa.edu/synaptic-vesicles); polyclonal anti-MBP (maltose binding protein; New England Biolabs, https://www.neb.com/products/e8030-anti-mbp-antiserum); monoclonal anti-GST (glutathione S-transferase, Santa Cruz Biotechnology, http://www.scbt.com/datasheet-138-gst-b-14-antibody.html); monoclonal anti-calmodulin (Sigma, http://www.sigmaaldrich.com/catalog/product/sigma/c3545?lang=en&region=US); monoclonal anti-HA (Roche Diagnostics, http://www.roche-applied-science.com/shop/products/anti-ha-biotin-high-affinity-3f10-); monoclonal anti-cortactin (Millipore, http://www.millipore.com/catalogue/item/05-180); monoclonal anti-sodium/potassium ATPase (Thermo Scientific, http://www.pierce-antibodies.com/Sodium-Potassium-ATPase-alpha-3-antibody-clone-XVIF9-G10-Monoclonal–MA3915.html). Secondary antibodies used were: Cy3 donkey anti-mouse IgM (Jackson ImmunoResearch, http://www.jacksonimmuno.com/Catalog/catpages/whol-mse.asp); Alexa-Fluor-488 and -594 donkey anti-rabbit and goat anti-mouse IgG (Molecular Probes, http://products.invitrogen.com/ivgn/en/US/adirect/invitrogen?cmd=catDisplayStyle&catKey=97901&filterDispName=Alexa+Fluor%26reg%3B&filterType=1&OP=filter&filter=ft_1601%2Ff_2101*&_bcs_=H4sIAAAAAAAAAMWP20rEMBCGnyY3FkvagNteVsuKCCIueh%2FT2XagSUoybenbO62HFV28FYYZ5vz9%0Al5mQxWPwzWgoJiK%2FSg4QJjQQ%2F6h3RINQlcj3bPM8p%2BgmpOBbcKnxlosRCTiMkR04dp23kHZke14X%0AuVpNFhRGWHO5kxwymfFguZMyu%2BC0coSvvkHY3mvLH68ZwnjX6LAkNRAYQu%2BSJ9D8mH6BDR%2F0P%2BlU%0AVUhu49S6T7rnAzvdYOCTa%2BtrQai9sY1Q9d3L7YPRVGMcer3caILWh4XBuHgPC09s4N%2FVHXUfz8vb%0AYvku86ToJPjflZTnlbwB4%2F0dHi0CAAA%3D); horseradish peroxidase (HRP)-conjugated goat anti-mouse and anti-rabbit (Bio-Rad http://www.bio-rad.com/en-us/product/hrp-conjugates); HRP-conjugated goat anti-rat (Invitrogen, http://tools.invitrogen.com/content/sfs/manuals/819520_Rev1008.pdf).

Chicken embryos

Embryonated White Leghorn chicken eggs were obtained from the University of Connecticut Poultry Farm (Storrs, CT) or Charles River Spafas. Embryos were kept at 37 °C in forced air-draft humidified incubators until embryonic day (E) 12–20.

Immunolabeling

Cochlear ducts were dissected from E19–20 chicken embryos. For SK2 immunolabeling, cochleae were fixed for 1 h in 2% paraformaldehyde at 4 °C, cryoprotected by immersion in increasing concentrations of sucrose, and embedded in 7.5% gelatin with 15% sucrose. For S-SCAM and α-actinin immunolabeling, cochleae were fixed in 4% paraformaldehyde with 15% picric acid, cryoprotected, and embedded in TissueTek OCT compound (Electron Microscopy Sciences, http://www.emsdiasum.com/microscopy/products/histology/embedding.aspx). Ten-micrometer thick cryosections were blocked with 5% normal donkey serum (Jackson Immunoresearch, http://www.jacksonimmuno.com/Catalog/CatPages/normal.asp) or 0.25% teleost gelatin (Sigma, http://www.sigmaaldrich.com/catalog/product/sigma/g7765?lang=en&region=US in PBS. Sections were incubated with primary antibodies for 1 h at RT, rinsed 3 times with blocking buffer, incubated with secondary antibodies for 45 min, rinsed, and mounted with coverslips using Vectashield (Vector Labs, http://www.vectorlabs.com/catalog.aspx?prodID=428).

Image analysis

Epifluorescence images were captured using a Zeiss Axioskop epifluorescence microscope and QImaging Retiga 200R CCD camera and analyzed using Nikon Instruments NIS Elements software. Confocal images were captured using a Leica TCS SP2 confocal microscope with HeNe (633 nm), Kr (568 nm), and Ar (488 nm) lasers and a 63 x 1.32 numerical aperture lens. Optical sections were taken in 0.5 μM steps. For each cell, 3 consecutive sections through a representative region were compressed for analysis. For labeled cochlea sections, epifluorescence images or confocal stacks from representative cells were used to assess co-localization of double-labeled proteins. Pixel intensities were measured along ~3 μM vertical lines drawn across representative regions of the efferent olivocochlear synapse that were distinguished by clearly detectable markers of the presynaptic terminal or postsynaptic membrane at the basal synaptic pole of the short hair cells. This criterion distinguished the synapse and verified the penetration of antibodies to the region. Presynaptic vs. postsynaptic localization of the test protein was defined on the basis of the extent of overlap of the peak pixel intensity with that of the marker pre- or postsynaptic protein and on the juxtaposition (predominantly red and green staining) vs. overlap (yellow staining) of the fluorescent double labeling.

RT-PCR and α-actinin sequencing

Total RNA was isolated from E19 chicken cochlear ducts using TRIzol Reagent (Invitrogen, http://products.invitrogen.com/ivgn/product/15596026). Reverse transcription (RT) was performed using oligo (dT) primers and SuperScript II reverse transcriptase (Invitrogen, http://prod-

ucts.invitrogen.com/ivgn/en/US/adirect/invitrogen?cmd=catDisplayStyle&catKey=101&filterDispName=SuperScript%26trade%3B+II+Reverse+Transcriptase&filterType=1&OP=filter&filter=ft_1201%2Ff_148201*&_cs_=H4sIAAAAAAAAAH2LQQqAIBBFTzMrSUwh3LZpHXQEG1JIDR31%2Bk0XCB7%2FwYM%2FzaDsXvLZHFUBehEH%0Alh4c1p%2FuiR4wK%2BiNGWPIkHqgki9M0uXIsQZCVqs8mHh8jig9xZvvoM2HslQasl6iPti8hAAAAA%3D%3D). PCR amplification was performed using primers common to chicken skeletal muscle, smooth muscle, and non-muscle α-actinin isoforms: 5'GACAACAAGC ACACCAACTA CACCATGGAGCA3' (forward), 5'ATCTGCTGTT TCCCGGGACA TGAAGTCAATGAAGG3' (reverse). PCR product of the expected size was extracted from agarose gel and sequenced.

SK2-ARK splice variant quantification

Total RNA isolated from chicken cochlear ducts at selected developmental ages was used for RT-PCR as described above, using SK2-specific primers flanking the ARK splice insertion site: 5'ACTTACGGAT CCAATTTCAT GATGGACACCCA3' (forward), 5'CATGTATGAC ATGATCTCTG CTCGAGTCAGTA3' (reverse). PCR products were subcloned into pcDNA3.1 (Invitrogen, http://tools.invitrogen.com/content/sfs/vectors/pcdna3.1-.pdf) and grown on LB-ampicillin plates. SK2 clones were amplified by PCR from individual colonies, and PCR products were digested with the restriction enzyme Hpy188I (New England Biolabs, https://www.neb.com/products/r0617-hpy188i), which recognizes a unique site in the ARK containing, but not the ARK lacking, splice variant. Presence or absence of digestion products was assessed by agarose gel electrophoresis. Identity was verified by sequencing of randomly selected clones. A total of 150–180 subclones were analyzed for each developmental age.

Q-PCR of Mouse Forebrain SK2 splice variants

Total RNA was extracted (Qiagen, http://www.qiagen.com/Products/Catalog/Sample-Technologies/RNA-Sample-Technologies/Total-RNA/RNeasy-Mini-Kit) from the cortex and hippocampus of young (postnatal day 8) and adult (3 mo old) mice. cDNA was generated using reverse transcription (Life Technologies) with oligo (dT) primers. Q-PCR assays employed SYBR Green (Life Technologies. http://products.invitrogen.com/ivgn/product/4367659?ICID=cvc-sybr-realtime-c1t1) and SK2 isoform primer sets: 5' GGAAATTCTT GCAAGCTATT CATCAATT3'(fwd), SK2-ARK,5' CAAGCTATTC ATCAAGCTCG GAAA3'(fwd), common reverse 5' TGGGTCTTTG CCAGATCCACTA3', and, as control, GAPDH 5' AGGTCGGTGT GAACGGATTTG3'(fwd),5'TGTAGACCAT GTAGT TGAGGTCA3' (rev).

Protein expression in *Xenopus laevis* oocytes

Full-length cDNAs: chicken SK2 and SK2-ARK (GenBank accession number NM_204798; gift from Paul Fuchs, Johns Hopkins University), chicken α9- and α10-nAChR subunits (HA-tag added to α10 C-terminus) (NM_204760 and XM_428183; gift from Ana Belén Elgoyhen, the Institute for Genetic Engineering and Molecular Biology (CONICET), and human α-actinin-1 (97% homology to chicken α-actinin-1) (NM_001130004; gift of David Critchley, University of Leicester) were cloned into the pOx oocyte expression vector. In vitro cRNA synthesis was performed using the mMessage mMachine T3 transcription kit (Applied Biosystems, http://products.invitrogen.com/ivgn/product/AM1348). Oocytes (provided by Joel Richter, University of Massachusetts Medical School) were obtained from adult *Xenopus laevis* frogs and defolliculated in OR2 (in mM: 82.5 NaCl, 2 KCl, 0.5 $MgCl_2$, 5 HEPES pH 7.6) containing 2mg/ml collagenase (Sigma) and 1mg/ml dispase II (Roche Applied Science, http://www.roche-applied-science.com/shop/products/dispase14301-ii-neutral-protease-grade-ii-). Oocytes (Stage V) were microinjected with cRNAS: 14–15ng each of α9-nAChR and α10-nAChR-HA, 10–14ng of α-actinin-1, and 3–8ng of SK2 or SK2-ARK. Oocytes were maintained at 19 °C for 2–3 d in ND96 (in mM: 96 NaCl, 2 KCl, 1 $MgCl_2$, 1.8 $CaCl_2$, 5 HEPES,pH 7.6) supplemented with 2.5mM sodium pyruvate, 50μg/ml tetracycline, 50 μg/ml gentamicin, 100μg/ml amikacin, and 100μg/ml ciprofloxacin (all from Sigma).

Electrophysiology

cRNAs encoding the chicken SK2 and SK2-ARK subunits were microinjected (3ng) into Stage V *Xenopus laevis* oocytes. SK2 currents were recorded under voltage clamp from the oocytes between 2 and 5 d after injection. Recordings were made in the inside-out patch-clamp configuration using an Axon 200B patch-clamp amplifier, and a Macintosh-based computer system running PatchMaster Software (HEKA Inc.). Patch pipettes were made of borosilicate glass and had resistances of between 1 and 1.5 Mohms in our standard internal and external solutions.

The internal (bath) solution contained in mM: 140 $KMeSO_3$, 20 HEPES, 2 KCl, 1 EGTA and $CaCl_2$ as needed (see below). The external (pipette) solution contained in mM: 140 $KMeSO_3$, 20 HEPES, 2 KCl, and 2 $MgCl_2$. After patch excision, solutions containing differing concentrations of free Ca^{2+} were superfused onto the cytoplasmic face of each patch using a DAD12 (ALA Scientific Instruments) sewer-pipette style superfusion system. Solutions were exchanged in less than 1 s.

During each experiment a voltage step from 0 to +50 mV was applied for 20 ms 5 times consecutively. The resulting five current responses were averaged before analysis. Current responses were recorded from each patch at the following Ca^{2+} concentrations in μM: 0.01, 0.1, 0.2, 0.5, 0.7, 1, 3, and 10. Ca^{2+} solutions were prepared by adding to our standard internal solution, which contained 1 mM EGTA, the correct amount of $CaCl_2$ (100 mM Orion Standard), as calculated with MaxChelator Software (http://maxchelator.stanford.edu/) to achieve the desired free [Ca^2]. We assumed our standard internal solution contains 10 μM total Ca^{2+} when no Ca^{2+} was intentionally added, as measured previously.[46] The amplitude of the SK2 current was measured as the difference between the current observed at 0 mV and that observed at +50 mV at the center of the voltage step. The difference in amplitude ΔI was then used to plot Ca^{2+} dose-response curves for each patch. Each curve was then fitted with

the Hill equation[47] below and normalized to the maximum of the fit:

$$\Delta I = \Delta I_{Min} + \underline{\Delta I_{Max}[Ca]^{H}}$$

$$[Ca]^{H} + KD^{H}$$

Here ΔI_{Min} and ΔI_{Max} are the minimum and maximum of the curve respectively. *KD* is the $[Ca^{2+}]$ at half-maximal response, and *H* is the Hill coefficient. Normalized dose-response curves from patches expressing the same channel type were then averaged to produce dose-response curves.

Recombinant peptide binding assays

Maltose binding protein (MBP) fusions of chicken SK2 and SK2-ARK C-termini (aa 368–553) were created by cloning sequence verified PCR products into the pMalC2 vector (New England Biolabs). Glutathione S-transferase (GST) fusion of full-length human α-actinin-1 was created by cloning into the pGex4T3 vector (GE Healthcare, https://www.gelifesciences.com/gehcls_images/GELS/Related%20Content/Files/1314716762536/litdoc28-9545-52PS_AA_06-2009_WEB_20110830172010.pdf). Fusion peptides were expressed in Rosetta-gami 2(DE3) cells (EMD Chemicals, http://www.emdmillipore.com/life-science-research/rosetta-gami-2de3-competent-cells-*/EMD_BIO-71351/p_wJab.s1O2lsAAAEjRxl9.zLX) and grown in LB media containing 0.5M NaCl and 2.5 mM betaine to an optical density (OD) of 500–700. Peptide expression was induced with 1mM isopropyl β-D-thiogalactopyranoside (IPTG) for 3 h at room temperature or for 18 h at 19 °C. Peptides were purified from bacterial lysates using GST-sepharose or amylose resin.

For binding assays, equal quantities of SK2- or SK2-ARK-MBP peptides were bound to amylose resin and incubated with α-actinin-1-GST in Tris-Tx buffer (in mM: 10 Tris pH 7.6, 50 NaCl, 5 EDTA, 30 $Na_4P_2O_7$, 50 NaF, 0.4 Na_3VO_4, 1% Triton X-100) supplemented with protease inhibitor cocktail (Thermo Scientific, http://www.piercenet.com/browse.cfm?fldID=02040806) and phosphatase inhibitor cocktail (Roche Applied Science, http://www.roche.com/products/product-details.htm?type=product&id=111). Beads were washed 3 times with Tris-Tx buffer. Complexes were eluted, separated on SDS-PAGE gels, and transferred to nitrocellulose membranes. Pulldown of α-actinin-1-GST was detected using anti-GST antibody, ECL Plus detection system (GE Healthcare, discontinued) and LAS-4000 imaging system (Fujifilm Life Sciences). The imager denotes saturated signals and care was taken to only use blots that were not saturated for quantification. SK2- or SK2-ARK-MBP peptides were also used to pull down equimolar amounts of purified bovine brain calmodulin (EMD Chemicals). Bound proteins were separated by SDS-PAGE and transferred to PVDF membranes. Membranes were fixed in 0.2% glutaraldehyde for 1 h before immunoblotting with anti-CaM antibody. Specificity controls included pulldown of GST with SK2- or SK2-ARK-MBP, and pulldown of α-actinin-1-GST or CaM by MBP. Band densities were quantified using Nikon Instruments NIS Elements software and normalized to SK2 or SK2-ARK levels, detected with anti-MBP antibody, in the same lane. In each experiment, normalized levels of α-actinin-1-GST or CaM co-precipitated with SK2-ARK-MBP were calculated as a percentage of co-precipitation with SK2-MBP (100%).

For α-actinin-1/CaM competition assays, SK2- or SK2-ARK-MBP were incubated with amylose resin and α-actinin-1-GST in Tris-Tx buffer. To assess the effects of Ca^{2+}, Tris-Tx buffer was supplemented with 5mM BAPTA or 1mM $CaCl_2$.[28,48] Bound complexes were washed, and CaM added at 0, 0.5, 1, or 10μM. Alternatively, SK2 or SK2-ARK peptides and amylose resin were incubated first with 10μM CaM in BAPTA or $CaCl_2$ buffer, washed, and then incubated with α-actinin-1-GST. Proteins were eluted and α-actinin-1-GST pulldown was assayed as above.

Co-immunoprecipitation from cochlear membrane fractions

Membrane fractions were prepared from E19–20 chicken cochlear ducts. Tissue was homogenized on ice in sucrose buffer (in mM: 320 sucrose, 10 HEPES, 1 EGTA) with protease inhibitor cocktail and centrifuged at approximately 2,000 x g for 10 min. The supernatant was centrifuged at 100,000 x g for 1 h, and the resulting membrane pellet was resuspended in membrane buffer (in mM: 190 NaCl, 10 KCl, 1 EGTA, 10 HEPES pH 7.4) with protease inhibitors. The suspension was sonicated and centrifuged again at 100,000 x g for 30 min to remove insoluble material. The supernatant was pre-cleared for 1 h with protein G agarose beads (Roche Applied Science) and incubated overnight at 4 °C with 8 μg of anti-SK2 antibody. Immunocomplexes were precipitated with protein G agarose beads and washed 6 times with membrane buffer supplemented with 0.1% Triton X-100. Proteins were eluted, separated on SDS-PAGE gels, and immunoblotted using anti-α-actinin-1 antibody, ECL Plus detection, and exposure to X-ray film. As a specificity control, equivalent membrane fractions were immunoprecipitated with 8μg anti-HA antibody. In some experiments, 5mM BAPTA was added to all buffers.

Co-immunoprecipitation from oocytes

Xenopus oocytes were injected with cRNAs encoding SK2 or SK2-ARK, HA-tagged α10, α9, and α-actinin-1 as above. To show dependence of co-precipitation on exogenous SK2, this cRNA was excluded in separate oocyte injections. Membrane fractions were used for SK2 immunoprecipitation at 3days after injection. Oocytes (45–75 for each prep) were homogenized in ice cold buffer H (in mM: 83 NaCl, 1 $MgCl_2$, 5 EDTA, 5 EGTA, 10 HEPES pH 7.8, 4–6μL/oocyte) and centrifuged for 10 min at 750 x g. Pellets were resuspended in buffer H and re-centrifuged. Combined supernatants were layered onto 7mL 15% sucrose in buffer H and centrifuged for 90 min at 160,000 x g. Membrane pellets were resuspended in Tris-Tx buffer, 2–4μL/oocyte, with protease and phosphatase inhibitors and incubated for 1 h at 4 °C with gentle agitation to solubilize membrane proteins. Insoluble material was removed by centrifugation at 100,000 x g for 1 h. Soluble proteins were pre-cleared with protein G agarose and incubated overnight with 6–9μg anti-SK2 antibody. Immunocomplexes were precipitated with protein G agarose beads, and washed 3 times with Tris-Tx buffer. Bound proteins were separated on SDS-PAGE gels and transferred to nitrocellulose membranes. Co-precipitation of HA-tagged α9/10-nAChRs and α-actinin-1 was assessed by immunoblotting. Band intensities were normalized to precipitated SK2 in the same

lane. In each experiment, normalized levels of α-actinin-1 or HA-tagged α9/10-nAChRs co-precipitated with SK2-ARK-MBP were calculated as a percentage of co-precipitation with SK2-MBP (100%).

For BAPTA-AM experiments, oocytes were incubated for 2 h at 19 °C with 50μM BAPTA-AM in ND96 or control ND96 before membrane fractionation. BAPTA (10mM) was added to all buffers used for BAPTA-AM-treated samples; for untreated controls, BAPTA and/or EGTA were omitted.

Surface biotinylation and endocytosis assay

Standard cell surface biotinylation assays[31,49] were used to measure surface expression and endocytosis of proteins expressed in oocytes. Three days after injection, oocytes were incubated for 30 min at 4 °C in 1mg/ml EZ-Link Sulfo-NHS-LC-Biotin (Thermo Scientific, http://www.piercenet.com/browse.cfm?fldID=01030901) to biotinylate surface proteins. Excess reagent was quenched by 3 washes in cold quench buffer (192mM glycine, 25mM TRIS-HCl in ND96). Biotinylated oocytes were incubated at 19 °C to allow endocytosis. Oocytes (34–40 per time point) were used to prepare membrane fractions, using 400μL volumes of buffer H. Membrane pellets were resuspended in ASB-14 buffer (in mM: 120 NaCl, 5 EDTA, 30 $Na_4P_2O_7$, 50 NaF, 50 TRIS-HCl pH 7.6, 0.1% ASB-14) with protease inhibitors and incubated overnight at 4 °C with gentle agitation. Insoluble material was removed by centrifugation at 16,000 x g for 30 min. Streptavidin-agarose beads (Thermo Scientific, http://www.piercenet.com/browse.cfm?fldID=01021103) were added to precipitate biotinylated proteins and washed 4 times in Tris-Tx buffer. Bound proteins were eluted and separated on SDS-PAGE gels. Levels of biotinylated SK2 and α9/10-nAChRs were assessed by immunoblotting and normalized to input membrane expression. Background precipitation from unbiotinylated samples was subtracted from each measurement. As a negative control, membranes were probed with antibodies against the intracellular actin-binding protein cortactin to confirm specific biotinylation of surface proteins only.

Disclosure of Potential Conflicts of Interest

No potential conflicts of interest were disclosed.

Acknowledgments

We thank Joel Richter, Chien-Ling Lin, and Morris Nehama of the University of Massachusetts Medical School for generously providing the *Xenopus laevis* oocytes, Paul Fuchs of Johns Hopkins University for the chicken SK2 clones, Ana Belén Elgoyhen of the Institute for Genetic Engineering and Molecular Biology (CONICET) for the chicken α9- and α10-nAChR subunit clones, David Critchley of the University of Leicester for the human α-actinin-1 clone, and Eric Frank of Tufts University for valuable discussions.

Funding

This work was funded by NIH NIDCD grants RO1 DC008802 to M.H.J., F31DC010114 to E.S., and the NINDS Tufts Center for Neuroscience Research (CNR) NINDS P30 NS047243.

References

1. Oliver D, Klöcker N, Schuck J, Baukrowitz T, Ruppersberg JP, Fakler B. Gating of Ca2+-activated K+ channels controls fast inhibitory synaptic transmission at auditory outer hair cells. Neuron 2000; 26:595-601; PMID:10896156; http://dx.doi.org/10.1016/S0896-6273(00)81197-6
2. Bond CT, Herson PS, Strassmaier T, Hammond R, Stackman R, Maylie J, Adelman JP. Small conductance Ca2+-activated K+ channel knockout mice reveal the identity of calcium-dependent afterhyperpolarization currents. J Neurosci 2004; 24:5301-6; PMID:15190101; http://dx.doi.org/10.1523/JNEUROSCI.0182-04.2004
3. Xu Y, Tuteja D, Zhang Z, Xu D, Zhang Y, Rodriguez J, Nie L, Tuxson HR, Young JN, Glatter KA, et al. Molecular identification and functional roles of a Ca(2+)-activated K+ channel in human and mouse hearts. J Biol Chem 2003; 278:49085-94; PMID:13679367; http://dx.doi.org/10.1074/jbc.M307508200
4. Köhler M, Hirschberg B, Bond CT, Kinzie JM, Marrion NV, Maylie J, Adelman JP. Small-conductance, calcium-activated potassium channels from mammalian brain. Science 1996; 273:1709-14; PMID:8781233; http://dx.doi.org/10.1126/science.273.5282.1709
5. Hirschberg B, Maylie J, Adelman JP, Marrion NV. Gating of recombinant small-conductance Ca-activated K+ channels by calcium. J Gen Physiol 1998; 111:565-81; PMID:9524139; http://dx.doi.org/10.1085/jgp.111.4.565
6. Roux I, Wersinger E, McIntosh JM, Fuchs PA, Glowatzki E. Onset of cholinergic efferent synaptic function in sensory hair cells of the rat cochlea. J Neurosci 2011; 31:15092-101; PMID:22016543; http://dx.doi.org/10.1523/JNEUROSCI.2743-11.2011
7. Johnson SL, Adelman JP, Marcotti W. Genetic deletion of SK2 channels in mouse inner hair cells prevents the developmental linearization in the Ca2+ dependence of exocytosis. J Physiol 2007; 583:631-46; PMID:17627990; http://dx.doi.org/10.1113/jphysiol.2007.136630
8. Murthy V, Maison SF, Taranda J, Haque N, Bond CT, Elgoyhen AB, Adelman JP, Liberman MC, Vetter DE. SK2 channels are required for function and long-term survival of efferent synapses on mammalian outer hair cells. Mol Cell Neurosci 2009; 40:39-49; PMID:18848895; http://dx.doi.org/10.1016/j.mcn.2008.08.011
9. Kong JH, Adelman JP, Fuchs PA. Expression of the SK2 calcium-activated potassium channel is required for cholinergic function in mouse cochlear hair cells. J Physiol 2008; 586:5471-85; PMID:18818242; http://dx.doi.org/10.1113/jphysiol.2008.160077
10. Galambos R. Suppression of auditory nerve activity by stimulation of efferent fibers to cochlea. J Neurophysiol 1956; 19:424-37; PMID:13367873
11. Brown MC, Nuttall AL. Efferent control of cochlear inner hair cell responses in the guinea-pig. J Physiol 1984; 354:625-46; PMID:6481647
12. Murugasu E, Russell IJ. The effect of efferent stimulation on basilar membrane displacement in the basal turn of the guinea pig cochlea. J Neurosci 1996; 16:325-32; PMID:8613799
13. Walsh EJ, McGee J, McFadden SL, Liberman MC. Long-term effects of sectioning the olivocochlear bundle in neonatal cats. J Neurosci 1998; 18:3859-69; PMID:9570815
14. Wersinger E, Fuchs PA. Modulation of hair cell efferents. Hear Res 2010; 279:1-12 PMID:21187136; http://dx.doi.org/10.1016/j.heares.2010.12.018
15. Maison SF, Luebke AE, Liberman MC, Zuo J. Efferent protection from acoustic injury is mediated via alpha9 nicotinic acetylcholine receptors on outer hair cells. J Neurosci 2002; 22:10838-46; PMID:12486177
16. Zheng XY, Henderson D, Hu BH, Ding DL, McFadden SL. The influence of the cochlear efferent system on chronic acoustic trauma. Hear Res 1997; 107:147-59; PMID:9165355; http://dx.doi.org/10.1016/S0378-5955(97)00031-2
17. Zheng XY, Henderson D, McFadden SL, Hu BH. The role of the cochlear efferent system in acquired resistance to noise-induced hearing loss. Hear Res 1997; 104:191-203; PMID:9119763; http://dx.doi.org/10.1016/S0378-5955(96)00187-6
18. Taranda J, Maison SF, Ballestero JA, Katz E, Savino J, Vetter DE, Boulter J, Liberman MC, Fuchs PA, Elgoyhen AB. A point mutation in the hair cell nicotinic cholinergic receptor prolongs cochlear inhibition and enhances noise protection. PLoS Biol 2009; 7:e18; PMID:19166271; http://dx.doi.org/10.1371/journal.pbio.1000018
19. Xia XM, Fakler B, Rivard A, Wayman G, Johnson-Pais T, Keen JE, Ishii T, Hirschberg B, Bond CT, Lutsenko S, et al. Mechanism of calcium gating in small-conductance calcium-activated potassium channels. Nature 1998; 395:503-7; PMID:9774106; http://dx.doi.org/10.1038/26758
20. Keen JE, Khawaled R, Farrens DL, Neelands T, Rivard A, Bond CT, Janowsky A, Fakler B, Adelman JP, Maylie J. Domains responsible for constitutive and Ca(2+)-dependent interactions between calmodulin and small conductance Ca(2+)-activated potassium channels. J Neurosci 1999; 19:8830-8; PMID:10516302

21. Schumacher MA, Rivard AF, Bächinger HP, Adelman JP. Structure of the gating domain of a Ca2+-activated K+ channel complexed with Ca2+/calmodulin. Nature 2001; 410:1120-4; PMID:11323678; http://dx.doi.org/10.1038/35074145
22. Fakler B, Adelman JP. Control of K(Ca) channels by calcium nano/microdomains. Neuron 2008; 59:873-81; PMID:18817728; http://dx.doi.org/10.1016/j.neuron.2008.09.001
23. Lu L, Zhang Q, Timofeyev V, Zhang Z, Young JN, Shin HS, Knowlton AA, Chiamvimonvat N. Molecular coupling of a Ca2+-activated K+ channel to L-type Ca2+ channels via alpha-actinin2. Circ Res 2007; 100:112-20; PMID:17110593; http://dx.doi.org/10.1161/01.RES.0000253095.44186.72
24. Ngo-Anh TJ, Bloodgood BL, Lin M, Sabatini BL, Maylie J, Adelman JP. SK channels and NMDA receptors form a Ca2+-mediated feedback loop in dendritic spines. Nat Neurosci 2005; 8:642-9; PMID:15852011; http://dx.doi.org/10.1038/nn1449
25. Vetter DE, Katz E, Maison SF, Taranda J, Turcan S, Ballestero J, Liberman MC, Elgoyhen AB, Boulter J. The alpha10 nicotinic acetylcholine receptor subunit is required for normal synaptic function and integrity of the olivocochlear system. Proc Natl Acad Sci U S A 2007; 104:20594-9; PMID:18077337; http://dx.doi.org/10.1073/pnas.0708545105
26. Vetter DE, Liberman MC, Mann J, Barhanin J, Boulter J, Brown MC, Saffiote-Kolman J, Heinemann SF, Elgoyhen AB. Role of alpha9 nicotinic ACh receptor subunits in the development and function of cochlear efferent innervation. Neuron 1999; 23:93-103; PMID:10402196; http://dx.doi.org/10.1016/S0896-6273(00)80756-4
27. Lee WS, Ngo-Anh TJ, Bruening-Wright A, Maylie J, Adelman JP. Small conductance Ca2+-activated K+ channels and calmodulin: cell surface expression and gating. J Biol Chem 2003; 278:25940-6; PMID:12734181; http://dx.doi.org/10.1074/jbc.M302091200
28. Lu L, Timofeyev V, Li N, Rafizadeh S, Singapuri A, Harris TR, Chiamvimonvat N. Alpha-actinin2 cytoskeletal protein is required for the functional membrane localization of a Ca2+-activated K+ channel (SK2 channel). Proc Natl Acad Sci U S A 2009; 106:18402-7; PMID:19815520; http://dx.doi.org/10.1073/pnas.0908207106
29. Bildl W, Strassmaier T, Thurm H, Andersen J, Eble S, Oliver D, Knipper M, Mann M, Schulte U, Adelman JP, et al. Protein kinase CK2 is coassembled with small conductance Ca(2+)-activated K+ channels and regulates channel gating. Neuron 2004; 43:847-58; PMID:15363395; http://dx.doi.org/10.1016/j.neuron.2004.08.033
30. Matthews TM, Duncan RK, Zidanic M, Michael TH, Fuchs PA. Cloning and characterization of SK2 channel from chicken short hair cells. J Comp Physiol A Neuroethol Sens Neural Behav Physiol 2005; 191:491-503; PMID:15868189; http://dx.doi.org/10.1007/s00359-005-0601-4
31. Rosenberg MM, Yang F, Giovanni M, Mohn JL, Temburni MK, Jacob MH. Adenomatous polyposis coli plays a key role, in vivo, in coordinating assembly of the neuronal nicotinic postsynaptic complex. Mol Cell Neurosci 2008; 38:138-52; PMID:18407517; http://dx.doi.org/10.1016/j.mcn.2008.02.006
32. Zhang M, Abrams C, Wang L, Gizzi A, He L, Lin R, Chen Y, Loll PJ, Pascal JM, Zhang JF. Structural basis for calmodulin as a dynamic calcium sensor. Structure 2012; 20:911-23; PMID:22579256; http://dx.doi.org/10.1016/j.str.2012.03.019
33. Waites GT, Graham IR, Jackson P, Millake DB, Patel B, Blanchard AD, Weller PA, Eperon IC, Critchley DR. Mutually exclusive splicing of calcium-binding domain exons in chick alpha-actinin. J Biol Chem 1992; 267:6263-71; PMID:1556133
34. Millake DB, Blanchard AD, Patel B, Critchley DR. The cDNA sequence of a human placental alpha-actinin. Nucleic Acids Res 1989; 17:6725; PMID:2780298; http://dx.doi.org/10.1093/nar/17.16.6725
35. Merrill MA, Malik Z, Akyol Z, Bartos JA, Leonard AS, Hudmon A, Shea MA, Hell JW. Displacement of alpha-actinin from the NMDA receptor NR1 C0 domain By Ca2+/calmodulin promotes CaMKII binding. Biochemistry 2007; 46:8485-97; PMID:17602661; http://dx.doi.org/10.1021/bi0623025
36. Glowatzki E, Fuchs PA. Cholinergic synaptic inhibition of inner hair cells in the neonatal mammalian cochlea. Science 2000; 288:2366-8; PMID:10875922; http://dx.doi.org/10.1126/science.288.5475.2366
37. Fuchs PA, Murrow BW. Cholinergic inhibition of short (outer) hair cells of the chick's cochlea. J Neurosci 1992; 12:800-9; PMID:1545240
38. Nie L, Song H, Chen MF, Chiamvimonvat N, Beisel KW, Yamoah EN, Vázquez AE. Cloning and expression of a small-conductance Ca(2+)-activated K+ channel from the mouse cochlea: coexpression with alpha9/alpha10 acetylcholine receptors. J Neurophysiol 2004; 91:1536-44; PMID:14657188; http://dx.doi.org/10.1152/jn.00630.2003
39. Lioudyno M, Hiel H, Kong JH, Katz E, Waldman E, Parameshwaran-Iyer S, Glowatzki E, Fuchs PAA. A "synaptoplasmic cistern" mediates rapid inhibition of cochlear hair cells. J Neurosci 2004; 24:11160-4; PMID:15590932; http://dx.doi.org/10.1523/JNEUROSCI.3674-04.2004
40. Saito K. Fine structure of the sensory epithelium of guinea-pig organ of Corti: subsurface cisternae and lamellar bodies in the outer hair cells. Cell Tissue Res 1983; 229:467-81; PMID:6839349; http://dx.doi.org/10.1007/BF00207692
41. Sridhar TS, Brown MC, Sewell WF. Unique postsynaptic signaling at the hair cell efferent synapse permits calcium to evoke changes on two time scales. J Neurosci 1997; 17:428-37; PMID:8987768
42. Reiter ER, Liberman MC. Efferent-mediated protection from acoustic overexposure: relation to slow effects of olivocochlear stimulation. J Neurophysiol 1995; 73:506-14; PMID:7760114
43. Sridhar TS, Liberman MC, Brown MC, Sewell WF. A novel cholinergic "slow effect" of efferent stimulation on cochlear potentials in the guinea pig. J Neurosci 1995; 15:3667-78; PMID:7751937
44. Beggs AH, Byers TJ, Knoll JH, Boyce FM, Bruns GA, Kunkel LM. Cloning and characterization of two human skeletal muscle alpha-actinin genes located on chromosomes 1 and 11. J Biol Chem 1992; 267:9281-8; PMID:1339456
45. Tuteja D, Rafizadeh S, Timofeyev V, Wang S, Zhang Z, Li N, Mateo RK, Singapuri A, Young JN, Knowlton AA, et al. Cardiac small conductance Ca2+-activated K+ channel subunits form heteromultimers via the coiled-coil domains in the C termini of the channels. Circ Res 2010; 107:851-9; PMID:20689065; http://dx.doi.org/10.1161/CIRCRESAHA.109.215269
46. Sweet TB, Cox DH. Measurements of the BKCa channel's high-affinity Ca2+ binding constants: effects of membrane voltage. J Gen Physiol 2008; 132:491-505; PMID:18955592; http://dx.doi.org/10.1085/jgp.200810094
47. Hill AV. The possible effects of the aggregation of the molecules of haemoglobin on its dissociation curves. J Physiol 1910; 40:iv-vii
48. Wang C, Wang HG, Xie H, Pitt GS. Ca2+/CaM controls Ca2+-dependent inactivation of NMDA receptors by dimerizing the NR1 C termini. J Neurosci 2008; 28:1865-70; PMID:18287503; http://dx.doi.org/10.1523/JNEUROSCI.5417-07.2008
49. Harris M, Garcia-Caballero A, Stutts MJ, Firsov D, Rossier BC. Preferential assembly of epithelial sodium channel (ENaC) subunits in Xenopus oocytes: role of furin-mediated endogenous proteolysis. J Biol Chem 2008; 283:7455-63; PMID:18195015; http://dx.doi.org/10.1074/jbc.M707399200
50. Ren Y, Barnwell LF, Alexander JC, Lubin FD, Adelman JP, Pfaffinger PJ, Schrader LA, Anderson AE. Regulation of surface localization of the small conductance Ca^{2+}-activated potassium channel, Sk2, through direct phosphorylation by cAMP-dependent protein kinase. J Biol Chem 2006; 281:11769-79; PMID:16513649; http://dx.doi.org/10.1074/jbc.M513125200